Self-Cleaning Cathodes for Endurance to Chromium Poisoning

upal@bu.edu

DOE Award #: DE-FE0031206

Final Report

Submitted to: U.S. Department of Energy, National Energy Technology Laboratory

Boston University Principal Investigator:

Prof. Uday Pal

(617) 353-7708

Project Duration: 10/01/2017 to 9/30/2021

Report Period: 10/01/2017 to 9/30/2021

Report Submitted: December 2021

Boston University DUNS #: 049435266

Boston University

881 Commonwealth Avenue

Boston, MA 02215 – 1300

X Uday Pal Digitally signed by Uday Pal Date: 2022.02.26 19:58:03 -05'00'

Uday Pal

Disclaimer

Table of Contents

Executive Summary

Chromium (Cr) poisoning remains a significant issue in long-term solid oxide fuel cell (SOFC) operation. While the addition of Cr in the interconnect and balance-of-plant (BOP) materials is effective in improving their resistance to oxidation, it also causes the deposition of resistive phases in the air electrode and thus cell performance loss. Previous work has investigated the mitigation of chromium deposition using getters, Cr diffusion resistant coatings, and more chromium-tolerant air electrode materials. However, these mitigation strategies merely postpone the degradation of performance due to Cr poisoning. Additionally, some strategies require the replacement of components, e.g., use of getters. Here we investigated a new, in-situ Cr poisoning mitigation strategy.

Based on the free energy minimization calculations, the most prevalent Cr vapor species concentration is CrO_3 in the absence of water vapor, and much higher concentrations of $CrO_2(OH)_2$, and $CrO_2(OH)$ vapor species in the presence of water vapor. The equilibrium cell potentials for the reduction of these oxide vapor species to the lower valent $Cr_2O_3(s)$ are all near 1.12 V at 800 °C, which is close to the open-circuit potential of the cell, indicating that the dissociation of Cr vapor species into lower valent oxides with the onset of current flow. Thus, the air electrode performance degradation caused by Cr-poisoning appears to be mostly associated with the Cr oxide vapor species dissociation at the electrochemically active sites in the air electrode. This was demonstrated in our earlier work, where we studied the mechanism of Cr-poisoning as a function of current density, humidity, microstructure, and distribution of electronic/ionic/mixed conducting oxide phases in the air electrode.

Our previous results have shown that when fuel electrode-supported SOFCs with $La_{1-x}Sr_xMnO_3$ (LSM)-based air electrodes and yttria-stabilized zirconia (YSZ) electrolyte were subjected to galvanostatic testing for 150 hours at 800 °C in contact with Crofer22APU/H mesh, under different air electrode atmospheres and current conditions, the performance degradation was most severe under galvanostatic conditions (increased with current) [1]. Introduction of water vapor (10%) in the air under galvanostatic conditions further increased the rate of performance degradation. In comparison, under open circuit conditions (no current) for 150 hours at 800 °C, the cell performance did not degrade in dry air nor when 10% water vapor was introduced in the air supply. The majority of Cr deposition was observed near the air electrode/electrolyte interface under galvanostatic conditions with 10% humidified air followed by dry air. Under open circuit conditions in dry air and 10% humidified air, Cr-containing oxide deposits were not detected in the air electrode. Thus, current appears to play a primary role and humidity with current an ancillary accelerating role in the Cr-poisoning phenomena suggesting an electrochemically-dominant degradation mechanism. Similar cell tests were also performed with fuel electrode supported SOFCs with YSZ electrolyte, Gd_2O_3 doped ceria (GDC) barrier layer and mixed ionic electronic $La_{1-x}Sr_xFeO_3$ (LSF)-based air electrodes (LSF-GDC active layer and LSF current collector) [2]. However, they showed negligible performance degradation during the 120 hours of galvanostatic testing. Microstructural investigation of the post-test LSF air electrodes indicated higher amounts of Cr- containing deposits on the electrode surface, much lesser amounts near the air electrode/electrolyte interface (compared to the LSM-based cells) and negligible amount in the bulk electrode. This indicates that the mixed conducting phases and their distribution determines the location and progression of the chromium deposit. If these deposits can be removed as vapor species it can extend the stable operating life of the air

electrode. Based on our observations that essentially no Cr-poisoning occurs when cell testing is stopped, two self-cleaning and performance recovery processes for the air electrode were proposed for this project: chemical cleaning and electrochemical cleaning.

In chemical cleaning, chromium oxide-containing deposits in the air electrode are allowed to volatilize as $CrO_2(OH)_2$, $CrO_2(OH)$, and CrO_3 vapors. The removal rate will depend on the form of the Cr-containing oxide deposit and its activity, which can be varied using changes to cell temperature and air humidity. In electrochemical cleaning, the chromium removal rate from the air electrode can be accelerated under an applied potential of < 100 mV with 5-20% H_2O (g) in the fuel, and 0-15% H_2O (g) in the air (mild electrolytic conditions). A more detailed discussion of the electrochemical cleaning process is provided in Task 6.

The chemical cleaning process is expected to be naturally slower than the electrochemical cleaning process. Further, since electrochemical cleaning was observed to be safe for continued cell operation, this project focused electrochemical cleaning. Overall, in this project we evaluated air electrode performance under conditions of chromium poisoning and electrochemical cleaning. Cell performance results were corroborated using post-test chromium quantification using energy dispersion spectroscopy (EDS).

Achievements of this project include:

1. Development of higher porosity air electrodes for more rapid Cr deposition and enhanced performance degradation (Task 2).
2. Demonstration of electrochemical cleaning using LSM-based cells employing a mild electrolytic bias condition (-15 mA/cm^2) with air containing 2-5% water vapor ($H_2O(g)$).

Changes in performance were compared using maximum power density (current-voltage curves) and corroborated by post-test Cr quantification using EDS. Scanning electron microscopy (SEM) imaging determined that Cr_2O_3 type deposits are removed as result of electrochemical cleaning, whereas Cr, Mn spinel deposits are not (Task 6).

3. Comparison of chromium content post-test utilizing SEM and EDS analysis, demonstrating Cr removal as a result of electrochemical cleaning. The chromium quantification procedure was refined to better capture Cr content present in the entirety of the cell (Task 7).
4. Demonstration of repeated electrochemical cleaning using LSM-based cells without effecting the stability of any of the fuel cell components. In conjunction with other poisoning mitigation strategies, we conclude that electrochemical cleaning can greatly improve the cell lifetime for LSM-based cells (Task 8).
5. Using our team's tests of chromium poisoning in other electrode materials, development of framework to understand Cr poisoning and cleaning for other MIEC-type electrodes (Additional Insights A).
6. Identification of another possible Cr poisoning mitigation method in LSM-based cells utilizing a thin covering of silver on the YSZ electrolyte surface due to its high oxygen solubility (Additional Insights B).

Task 1: Project Management and Planning

Project members have met as needed to discuss progress.

Task 2: Cell Fabrication

In this work, air electrodes were screen printed onto half cells that were commercially purchased from SOFCMAN Energy (Ningbo, China) (Figure 1). Half cells consisted of a 400 μm thick NiO-8YSZ (8 mol% Y_2O_3-92 mol% ZrO_2) fuel electrode substrate, a 7 μm thick NiO-8YSZ fuel electrode active layer, and a 7 μm thick dense YSZ electrolyte. Air electrode slurries were prepared before screen printing by mixing the desired electrode powders (LSM and YSZ) and ball milling with alpha-terpineol (Alfa Aesar), carbon black pore former (Fisher Scientific), and binder (V6, Heraeus). A 1:1 weight ratio of $(La_{0.8}Sr_{0.2})_{0.9}MnO_{3-\delta}$ (Fuel Cell Material) and 8YSZ (Tosoh Corp) powders was used for the air electrode active layer. LSM powder was used for the air electrode current collector layer. The two layers, each 25 μm thick, were screen printed on the electrolyte and sintered separately at 1200°C for two hours. The diameters of the NiO-YSZ substrate and air electrode were 3 cm and 1.6 cm, respectively.

The air electrodes were fabricated with much larger pores and grains (Fig 2.a) compared to commercially purchased full cells (Fig. 2.b). This facilitates Cr vapor flow to the air electrode/electrolyte interface where the majority of Cr deposition occurs for LSM-based cells (Figure 3). Furthermore, this more open design reduces the triple phase boundary (TPB) length. Therefore, we are able to decrease the duration of cell testing, as well as clearly distinguish

changes in cell performance as a result of changes in the concentration of Cr-containing deposits within the air electrode.

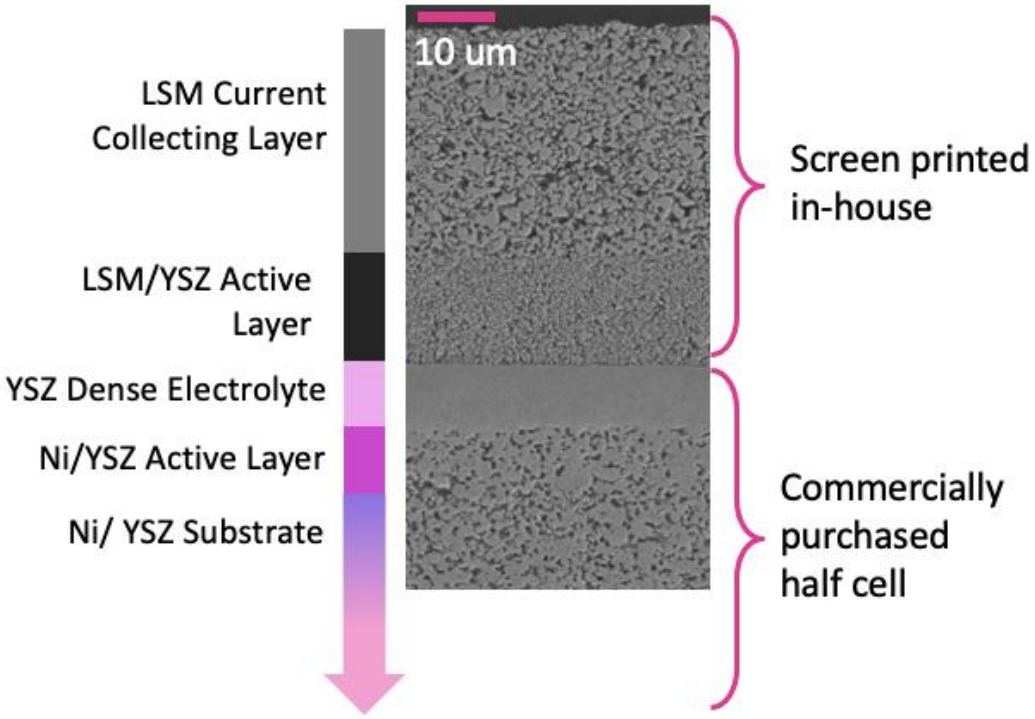

Figure 1. Cross sectional SEM micrograph of screen-printed, LSM-based cells.

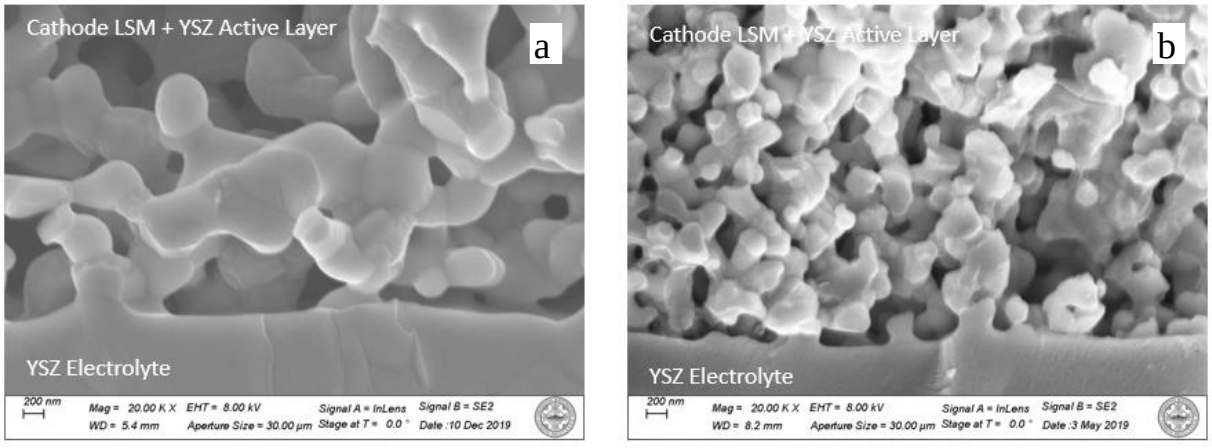

Figure 2. SEM images of (a) cells with in-house, screen-printed air electrodes and (b) commercially purchased full cells.

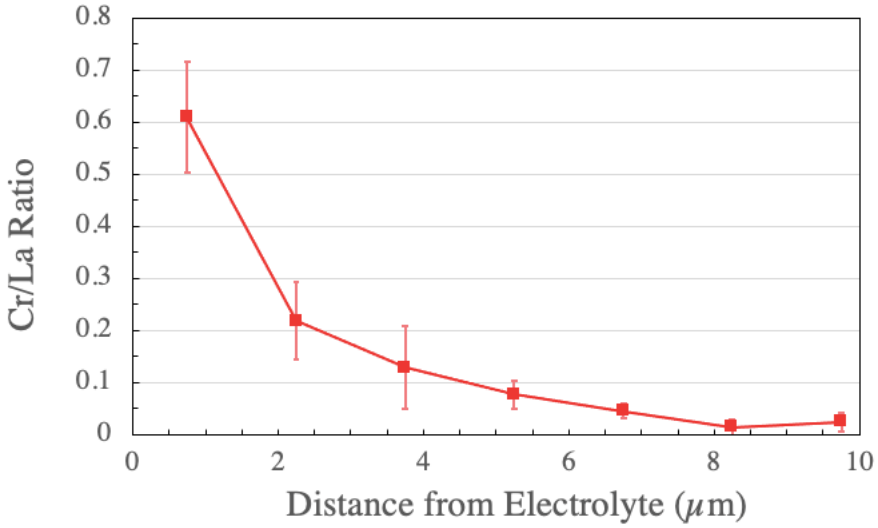

Figure 3. Chromium content as a function of distance from the electrolyte into the LSM air electrode demonstrating that the majority of Cr deposition occurs at the electrode/electrolyte interface.

Task 3: Fabrication of EPD Spinel Coated Crofer 22 APU/H Mesh

Previously, a porous $CuMn_2O_4$ spinel coating and a dense $CuMn_{1.8}O_4$ spinel coating on Crofer22 APU mesh were shown to reduce the rate of Cr poisoning [3]. Cu, Mn spinel phases were synthesized via the glycine nitrate route. Uniform coatings were deposited onto Crofer22 APU meshes by the EPD process. When tested against an uncoated Crofer 22 APU mesh, the rate of degradation as a result of Cr poisoning was greatly reduced for both cells in contact with the Cr, Mn spinel coated-Crofer22 APU meshes (Figure 4). (The increase in performance in the first 48 hours is a result of cell activation, which out competes the effects of poisoning in these tests.) The duration of a cell test demonstrating sufficient chromium poisoning and electrochemical cleaning for a cell in contact with a dense $CuMn_{1.8}O_4$ spinel-coated interconnect would be very lengthy and thus was determined to be outside the scope of our work. However,

we are confident that electrochemical cleaning in conjunction with the dense $CuMn_{1.8}O_4$ spinel-coated interconnect would significantly increase the cell lifetimes of LSM-based cells.

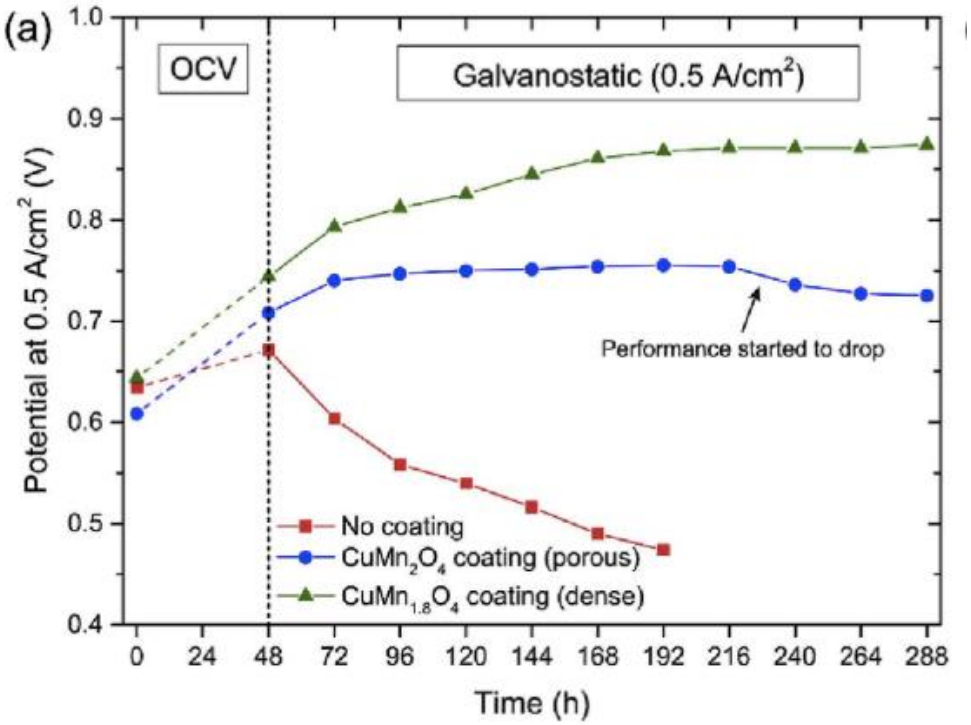

Figure 4. Potential measured at 0.5 A/cm^2 as a function of time operated at 800C, under dry air, 0.5 A/cm^2 for cells in contact with an uncoated Crofer22 APU mesh (red squares), a porous $CuMn_2O_4$ spinel-coated mesh (blue circles), and a dense $CuMn_{1.8}O_4$ spinel-coated mesh (green triangles). [3]

Task 4: Electrochemical Cell Test Setup and Testing

Before loading the cell into the test stand (Figure 5), silver mesh (Fuel Cell Materials) was attached using silver paste on the air side of the cell, and nickel mesh (Alfa Aesar) was attached using Ni paste on the fuel side. Both served as current collectors. The cell was

sandwiched between two alumina tubes, with a gold O-ring and mica gasket (Fuel Cell Materials) sealing the gas environments on either side. The outside of the tube was sealed using glass paste (Fuel Cell Store). Spring-loaded silver wire and nickel rods (Alfa Aesar) were used for electrical connection. Small Cr_2O_3 pellets (Alfa Aesar) were contained inside a silver mesh (Alfa Aesar) and attached to the end of a retractable ceramic tube, which supplied humidified air and vaporized chromium species to the air electrode during poisoning. During the poisoning phase, the Cr_2O_3 bundle was positioned ~1 cm from the air electrode in the hot zone to facilitate Cr vaporization.

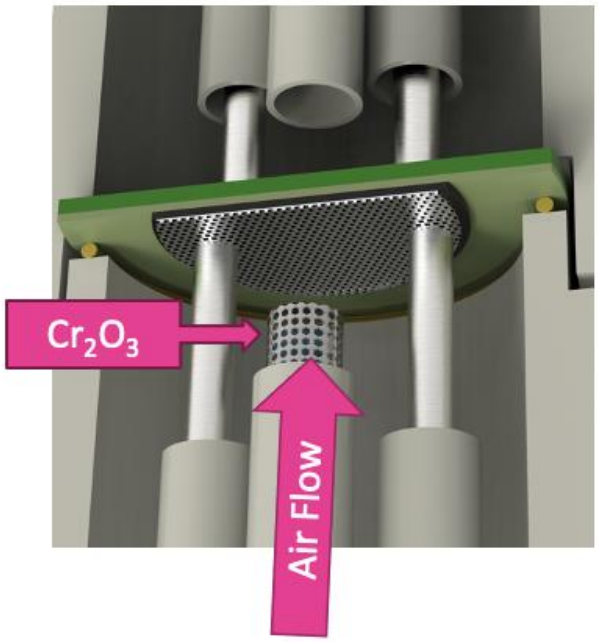

Figure 5. Cross-sectional schematic illustrating alumina housing with sealing, electrical contacts, and gas flows for full cell testing.

Here, we present current-voltage (I-V) curves to demonstrate changes to cell performance. (Although electrochemical impedance spectroscopy (EIS) measurements were also acquired, they corroborated the I-V measurements, and thus are not presented here.) I-V curves were acquired between each test phase to quantify changes in cell performance. All

measurements were acquired at 800°C, under dry air (air side) and 2% humidified hydrogen (fuel side). Sufficient time (~1 hour) was given before each I-V measurement to ensure cell equilibration. Electrochemical measurements were conducted using a Princeton Applied Research 263A PARSTAT®, KEPCO COP 20-20M power amplifier, and a Solartron SI 1250 frequency response analyzer.

Task 5: Self-cleaning of Electronic and MIEC Cathodes under Open Circuit Conditions – Chemical Cleaning

Chemical cleaning was initially proposed as a more benign and less aggressive alternative to electrochemical cleaning. Chemical cleaning relies on increasing the vapor pressures of Cr containing species by increasing the temperature and water vapor content in the air. For instance, having 5% humid air at 900 °C over Cr_2O_3 would provide a saturated partial pressure of 10^{-8} atm for the chromium vapor species. Therefore, with an airflow of 1 L/min, the maximum removal rate of Cr_2O_3 would be $9.5*10^{-4}$ mg/hr. The area of the air electrode is 2 cm^2 and the extent of poisoning that occurred (see Table 1 in the following section) yielded a 100nm thick layer of Cr_2O_3 over ¼ of the air electrode/electrolyte interface, i.e. $1.5*10^{-2}$ mg of Cr_2O_3 is deposited. It would take on the order of hundreds of hours to chemically clean this amount of chromium oxide deposit. However, electrochemical cleaning was found to have a much higher rate of Cr_2O_3 removal than would be possible by chemical cleaning and also since electrochemical cleaning did not degrade the cell under the electrolytic current utilized (see electrochemical cleaning), we focused on electrochemical cleaning.

Task 6: Self-cleaning of Electronic and MIEC Cathodes under Mild Electrolytic Conditions – Electrochemical Cleaning

The mechanism of electrochemical cleaning is based in the observation that Cr poisoning occurs with the onset of current flow in LSM-based cells (Figure 6) [1]. During electrochemical cleaning a mild electrolytic bias is applied in order to reverse the Cr deposition reactions:

$$2CrO_3(g, \text{air side}) + 3H_2(g, \text{fuel side}) \rightleftarrows Cr_2O_3(s, \text{air side}) + 3H_2O(g, \text{fuel side})$$

$$2CrO_2(OH)_2(g, \text{air side}) + 3H_2(g, \text{fuel side}) \rightleftarrows Cr_2O_3(s, \text{air side}) + 2H_2O(g, \text{air side}) + 3H_2O(g, \text{fuel side})$$

$$3CrO_2(OH)(g, \text{air side}) + 3H_2(g, \text{fuel side}) \rightleftarrows 1.5Cr_2O_3(s, \text{air side}) + 1.5H_2O(g, \text{air side}) + 3H_2O(g, \text{fuel side})$$

Reformation of the Cr vapor species frees up the active sites in the cells, restoring cell performance.

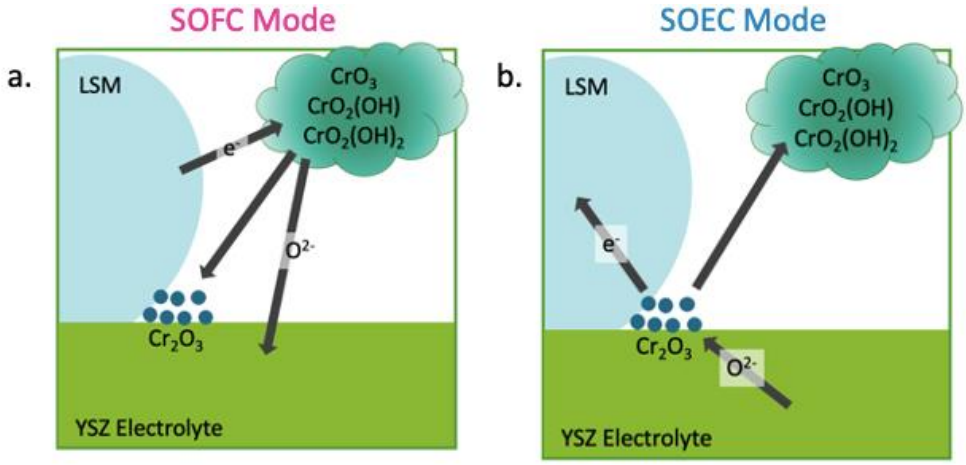

Figure 6. Mechanisms of Cr poisoning (a) and electrochemical cleaning (b) in LMS-based cells.

Demonstration of electrochemical cleaning was carried out with two cell tests [4]. Both the poisoning baseline cell (PB) and electrochemically cleaned cells (EC) were subjected to activation and poisoning phases (conditions provided in Table 1). At this point the poisoning baseline cell was cooled and characterized. The electrochemically cleaned cell was additionally subjected to cleaning for 2 hours. In both tests, the Cr source was introduced into the system only

during the poisoning phase. This allowed for the effects of activation, poisoning, and cleaning to be clearly distinguished.

Table 1. Test conditions for poisoning baseline (PB) and electrochemically cleaned (EC) cells.

Phase	Duration (h)	Temperature (°C)	Current Density (mA/cm^2)	Air Humidity (%)	Fuel Humidity (%)
Activation	48	800	500	0	2
Poisoning	120	800	500	5	2
Cleaning	2	800	-150	10	10

Current-voltage results demonstrate similar drops in performance as a result of poisoning (Figure 7). After two hours of electrochemical cleaning, EC cell demonstrates 67% recovery in cell performance, when comparing the maximum power densities. The result is corroborated by post-test Cr quantification using EDS which demonstrated a 78% reduction of Cr content as a result of electrochemical cleaning (Figure 8). A detailed explanation of Cr quantification is given in Task 7.

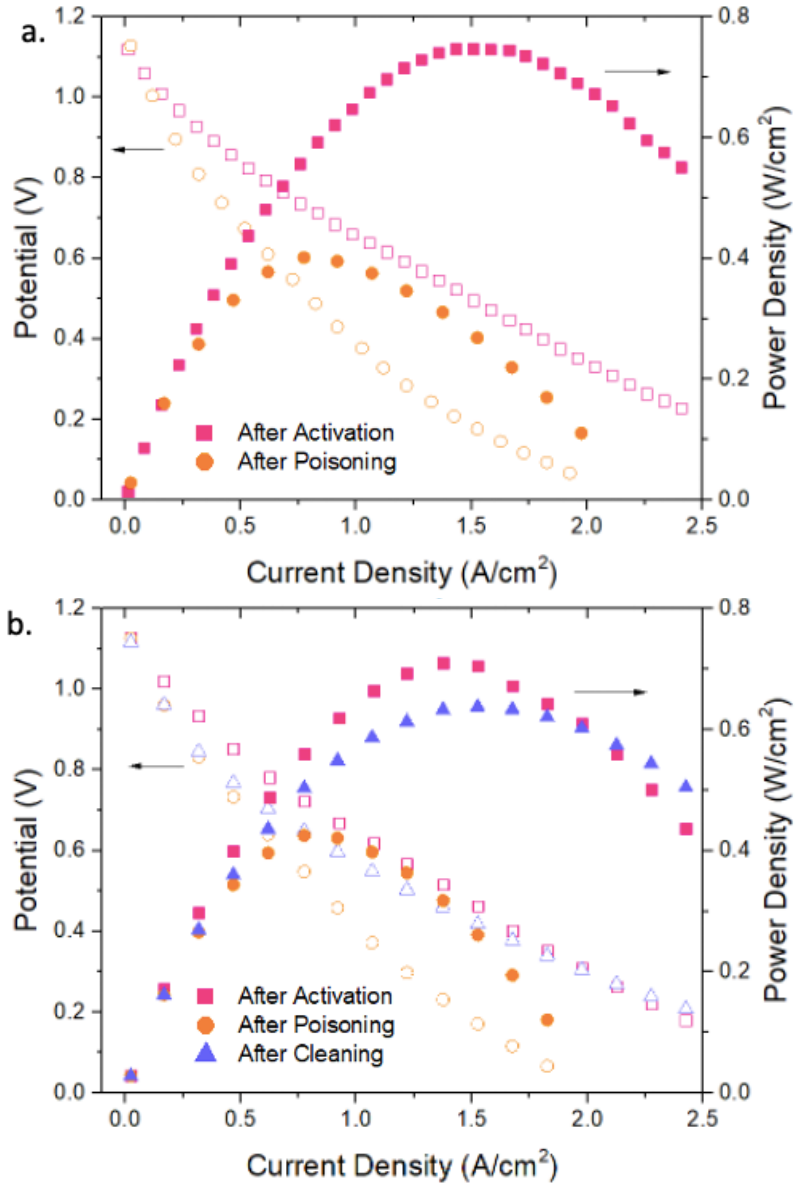

Figure 7. Current-voltage and power density curves of PB (a) and EC (b) tested cells.

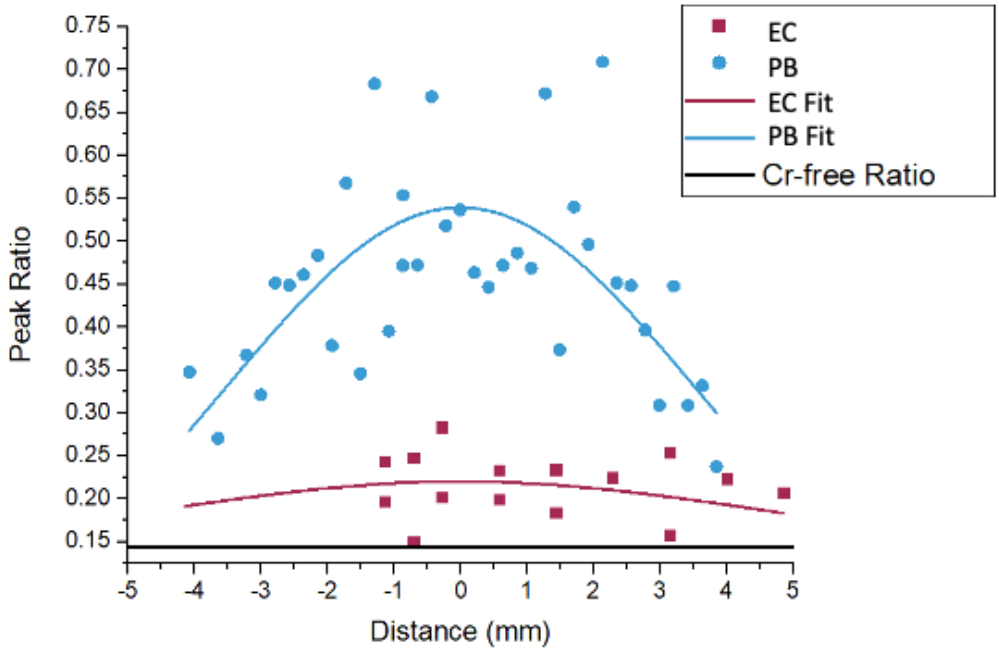

Figure 8. Chromium quantification as a function of distance along the air electrode/electrolyte interface EC and PC cells.

SEM imaging shows that in YSZ electrolyte surface in PB cell is covered with Cr deposits after 120 hours poisoning (Figure 9.a). Further, we observe two different deposit morphologies. The smaller, round deposits are identified as Cr_2O_3 (Figure 10.b) and the larger, faceted deposits as Cr, Mn spinel (Figure 10.c). Interestingly, SEM imaging demonstrates that electrochemical cleaning is effective at removing Cr_2O_3, whereas Cr, Mn spinel type deposits are unaffected (Figure 9.b).

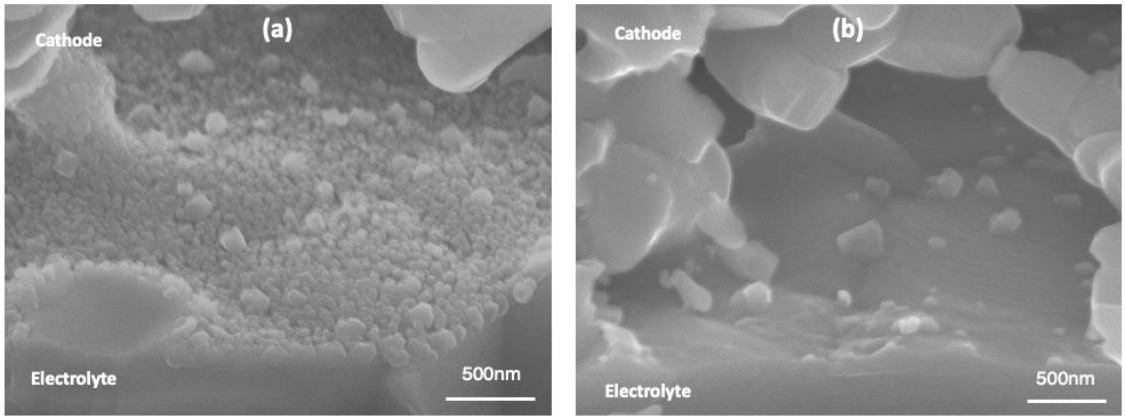

Figure 9. SEM micrograph of PB cell poisoned for 120 hours under 5% humidified air, 0.5 A/cm^2 at 800ºC (a) and EC cell poisoned under the same conditions followed by electrochemical cleaning for 2 hours under 10% humidified air, 10% humidified fuel, -0.15 A/cm^2 at 800ºC (b).

If we compare PB to another cell poisoned under the same conditions but for a shorter period of time, we observe that the Cr, Mn spinel does not start to appreciably form until sometime between 25 and 120 hours (Figure 11). This indicates that unlike Cr_2O_3, the formation of Cr, Mn spinel is chemical, and not electrochemical, in nature.

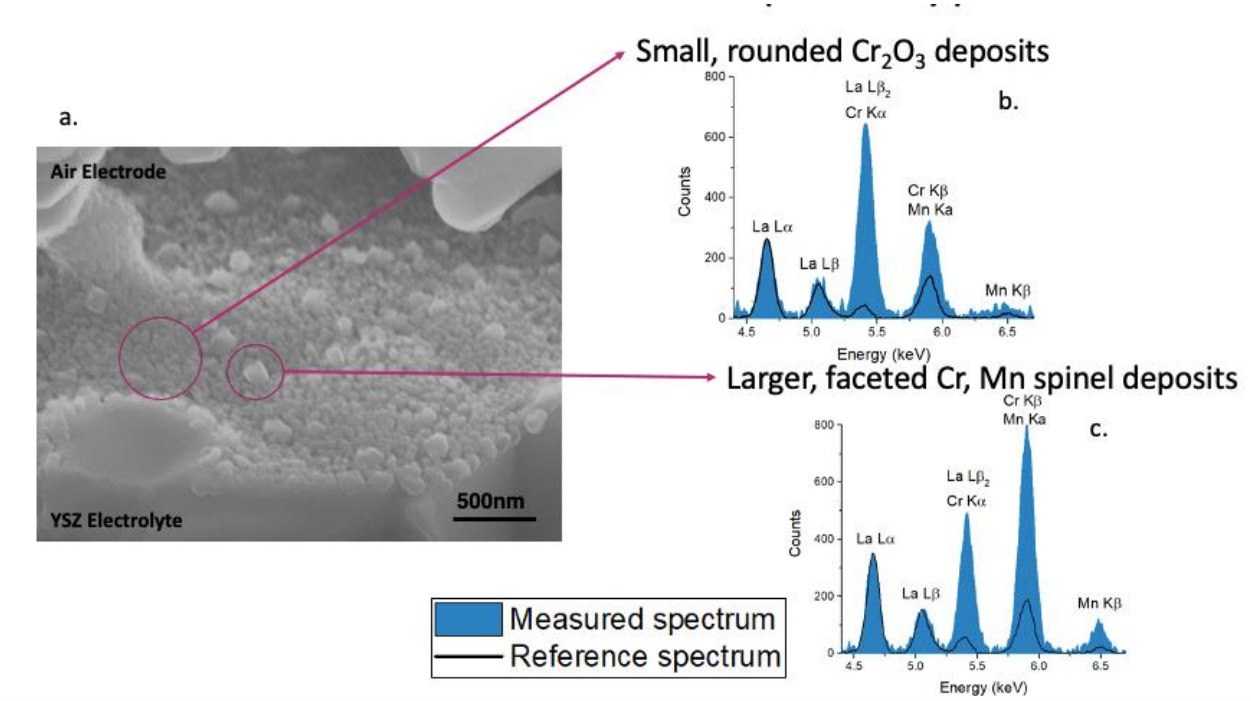

Figure 10. SEM micrograph of 120h poisoned cell (a) and EDS spectra for small, rounded deposits (b) and larger, faceted deposits (c).

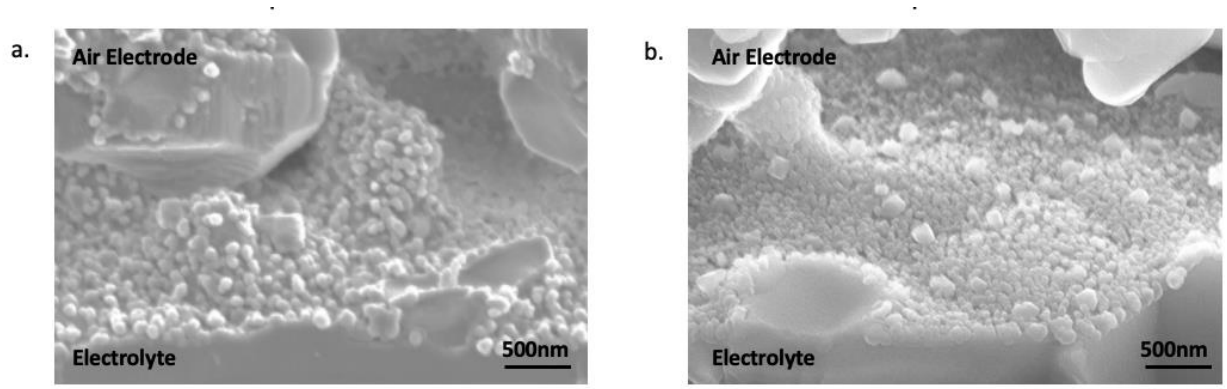

Figure 11. SEM micrographs of a cell poisoned for 25 hours under 5% humidified air, 0.5 A/cm^2 at 800ºC (a) and PB cell poisoned for 120 hours under 5% humidified air, 0.5 A/cm^2 at 800ºC.

This is slightly complicated by the follow mechanism of Mn ion migration in LSM-based cells. Under cathodic polarization, Mn ions migrate from the LSM phase into the YSZ electrolyte (Figure 12) [5]. At some point after appreciable Cr poisoning on the YSZ electrolyte surface, the

deposited Cr oxide reacts with Mn ions in the YSZ phase forming Cr, Mn spinel. This also explains why we observe Cr, Mn spinel a significant distance from the LSM phase across the YSZ electrolyte surface. Again, since Cr, Mn spinel is hypothesized to form via this mechanism (and does not start forming with the onset of current flow), it is not removed via electrochemical cleaning, as is Cr oxide.

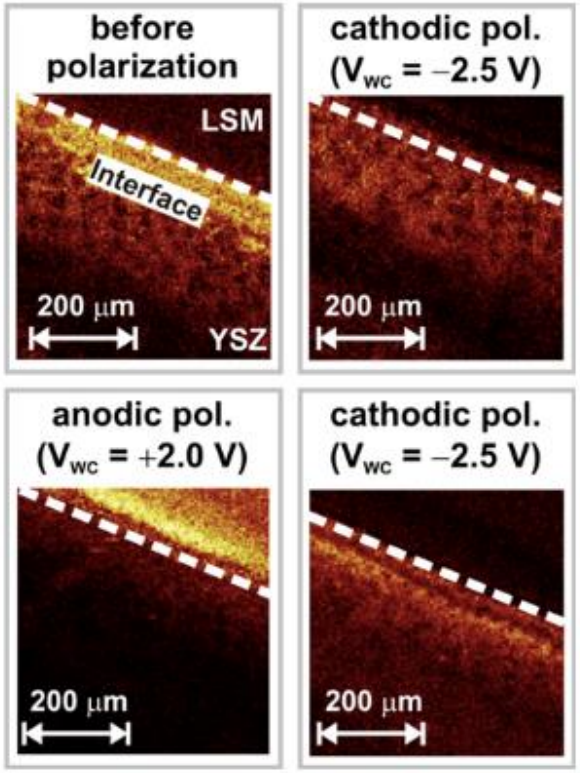

Figure 12. SIMS maps demonstrating migration of Mn ions into the YSZ phase under cathodic polarization and to the LSM phase under anodic polarization [5].

This process provides one explanation for the strong activation effect observed in the first couple of days in LSM-based cells (by increasing the electronic conductivity of the YSZ phase, and thus extending the TPB region for the oxygen reduction reaction). Thus, we also found over the course of this project that in order to isolate the improvement in cell performance as a result

of electrochemical cleaning, it was necessary to reactivate the cells after anodic bias. Leaving the cells in open circuit condition overnight was sufficient to reverse the effects of deactivation observed in LSM-based cells when operated in electrolysis mode. This reactivation effect resulted in, generally, an additional ~5% in performance recovery.

Of course, the simple solution to the fact that electrochemical cleaning is not effective at Cr, Mn spinel removal is to clean the cells prior to the formation of the spinel. Future works of this project include a diagnostic measurement to determine the onset of (appreciable) spinel formation. Further, another avenue of exploration is the decomposition of Cr, Mn spinel. In air, Cr, Mn spinel decomposes below ~480ºC (Figure 13.a). Thus, the idea is to cool down cells to below the decomposition temperature, allow the Cr, Mn spinel to decompose, heat back up to temperature, and then perform electrochemical cleaning on the deposited and decomposed Cr oxide. This process could be facilitated by increasing the pO_2 as this increases the decomposition temperature. Under pure oxygen, it is ~540ºC (Figure 13.b). This is of course important considering thermal cycling and time spent where the cell is not being operated.

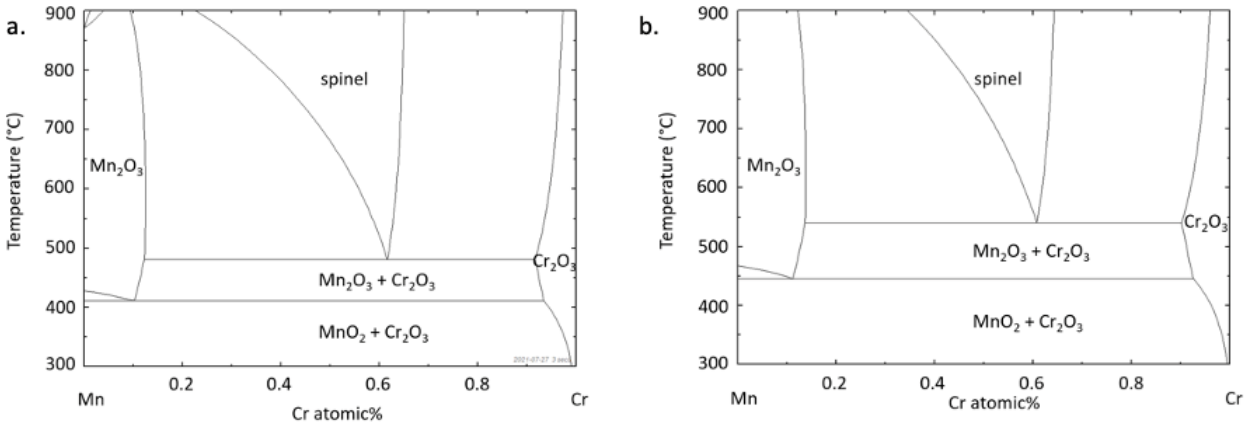

Figure 13. Cr/Mn compositional phase diagram as a function of temperature under air (pO_2 = 0.21) (a) and pure oxygen (b). Phase diagrams generated using FactSage.

Task 7: Quantitative Microstructural Characterization

Electrochemical measurements were corroborated with post-test Cr quantification using EDS analysis. Cells were fractured, mounted in cross-section in epoxy, polished, and sputter coated with carbon for quantitative analysis of the Cr concentration profile across the air electrode. Samples were examined using scanning electron microscopy (Zeiss Supra 55 VP) and energy dispersive spectroscopy (Oxford Instruments, High Wycombe, UK). The acquired EDS spectra were analyzed using AZtec software (Oxford Instruments, High Wycombe, UK). EDS area samples were acquired at the electrode/electrolyte interface where the majority of Cr deposition occurs for LSM-based cells (Figure 3). Area scans measured approximately 1.5 µm by 80 µm (Figure 14).

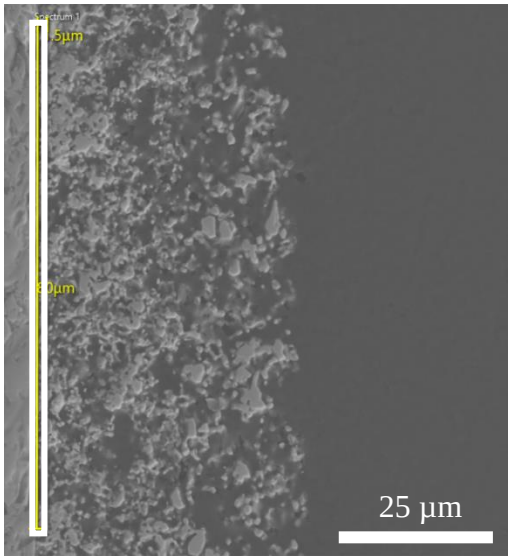

Figure 14. EDS area scans (1.5 µm by 80 µm) acquired at the air electrode/electrolyte interface for Cr quantification.

The ratio of peak intensities was used to compare between cells since the spectra for La and Cr have overlapping peaks (Figure 15). An elevation in III/I peak ratio over the Cr free ratio is indicative of the presence of Cr in the system:

$$\text{Cr Content Ratio} = \frac{\text{Cr } K\alpha + \text{La } L\beta_2}{\text{La } L\alpha}$$

$$= \frac{peak\ III}{peak\ \text{I}}$$

$$= 0.144 \text{ (Cr-free cell)}$$

Furthermore, an elevation in the V/I peak ratio over the standard LSM ratio is indicative of an enhance of Mn content in a region, which we attribute to the Cr, Mn spinel:

$$\text{Mn Content Ratio} = \frac{\text{Mn } K\beta}{\text{La } L\alpha}$$

$$= \frac{peak\ V}{peak\ \text{I}}$$

$$= 0.086 \text{ (Cr-free cell)}$$

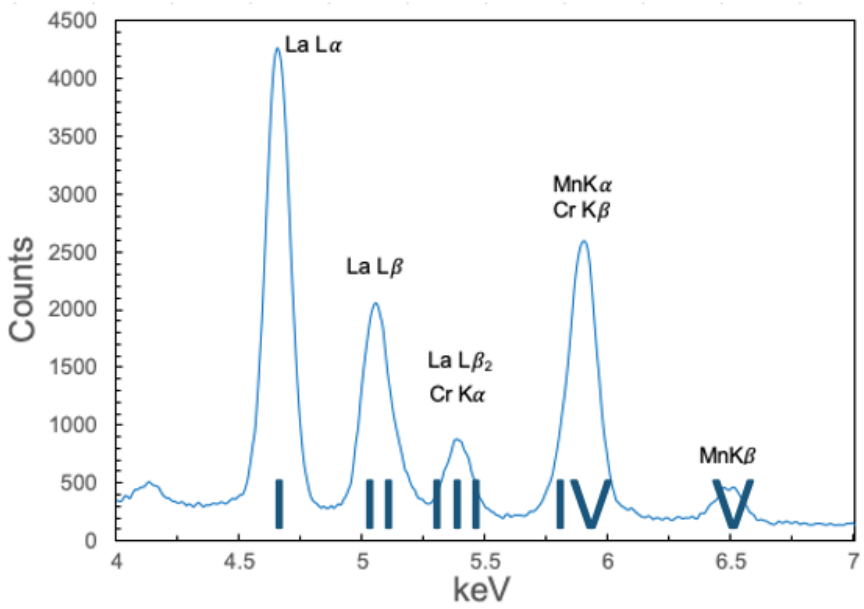

Figure 15. Example EDS spectrum highlighting signals used to calculate Cr and Mn ratios.

It was found that Cr content varies greatly across the cell as a function of the placement of the air inlet tube. Cr oxide pellets are placed inside the air inlet tube so that Cr containing vapor species are brought to the air electrode via the vapor phase (Figure 4). Thus, a more accurate depiction of Cr content in each cell is made by measuring the Cr/La peak ratio as a function of distance along the air electrode/electrolyte interface (Figure 16). This distribution can then be fit using a Gaussian distribution and integrated to compare values between cells.

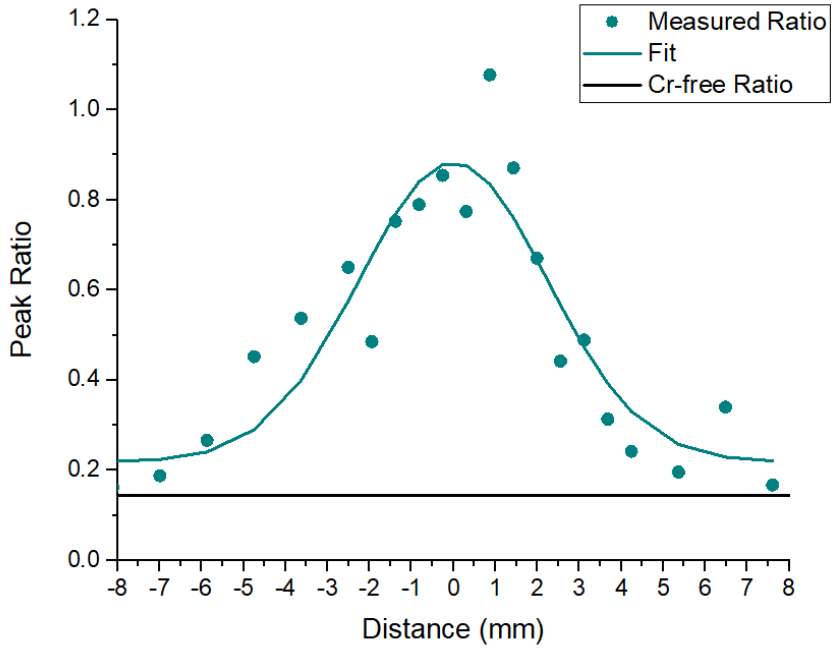

Figure 16. Gaussian curve fit of Cr quantification at the air electrode/electrolyte interface.

Task 8: Demonstrate at least two cycles of cleaning

Three single cell tests were conducted to demonstrate multiple poisoning-cleaning cycles [6]. These are designated as: multiple cycle poisoning baseline cell (MC-PB), multiple cycle

electrochemical cleaning cell (MC-EC), and electrochemical reference cell (MC-REF). Testing conditions are summarized in Table 2. Please note that cell stacks under industrial operating conditions were not tested as we did not have access to our collaborators (LG Fuel Cell went out of business in USA and Covid restrictions prevented us from contacting Fuel Cell Energy)

Table 2. Operating conditions for multiple cycle cleaning tests.

Phase	Duration (h)	Temperature (°C)	Current Density (mA/cm^2)	Air Humidity (%)	Fuel Humidity (%)
Activation	48	800	500	0	2
Poisoning	25	800	500	2	2
Cleaning	2	800	-150	5	10

All three cells were activated for 48 hours. MC-PB and MC-REF were exposed to Cr vapors for 25 hours during the poisoning phase. MC-PB was cooled down at this point. MC-EC was electrochemically cleaned for two hours. The poisoning and cleaning phases were repeated two more times for a total of three cycles.

MC-REF was conducted to confirm that cell degradation during the poisoning phase was caused entirely by exposure to the Cr-containing vapor species and that minimal damage was induced by running the cell in electrolytic mode during cleaning. MC-REF was exposed to identical conditions during the poisoning as MC-PB & MC-EC, but without the Cr source. This phase is referred hereon as SOFC exposure. The cell was then switched to the electrolytic (cleaning) mode with the same conditions as used for MC-EC for 2 hours (referred hereon as

SOEC exposure). After cleaning, MC-REF was activated overnight before being cooled to room temperature.

Figures 17 and 18 show the changes in performance for MC-PB and MC-EC, respectively. As a result of poisoning for 25 hours, both cells demonstrated a decrease in maximum power density, resulting in a 13% and 18% drop in performance, respectively.

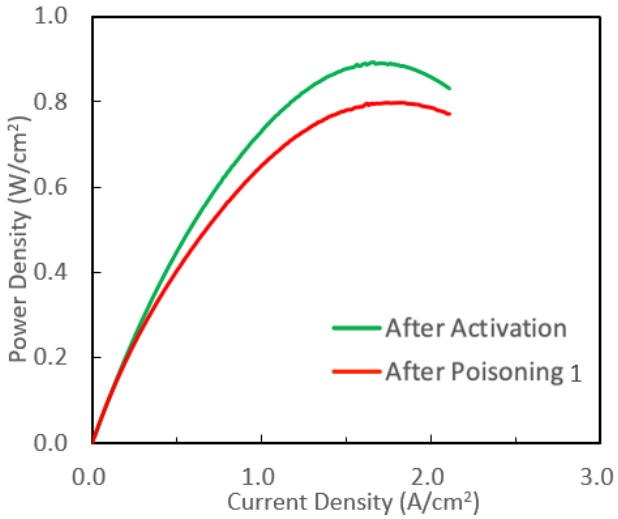

Figure 17. I-V curves of the poisoning baseline cell (MC-PB) after activation and after poisoning for 25 hours.

After the first cleaning cycle, the maximum power density of MC-EC increased to 0.80 W/cm^2 (Figure 18). The fact that the electrochemically cleaned cell exhibited better performance than before poisoning (but after activation) may be because activation is still ongoing during the poisoning process. After two additional poisoning-cleaning cycles, the maximum power density after cleaning remained the same, indicating that the electrochemical cleaning process is repeatable (Figure 19). This suggests that cells in stacks can be periodically electrochemically cleaned to recover the original cell performance prior to Cr poisoning.

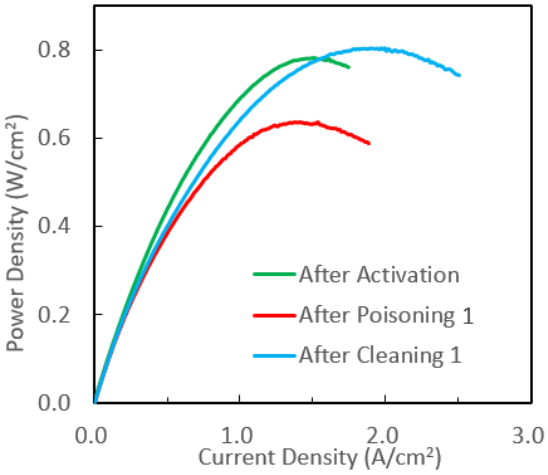

Figure 18. I-V curves for multiple cyclic electrochemical cleaning cell (MC-EC) after the first cycle of poisoning and cleaning.

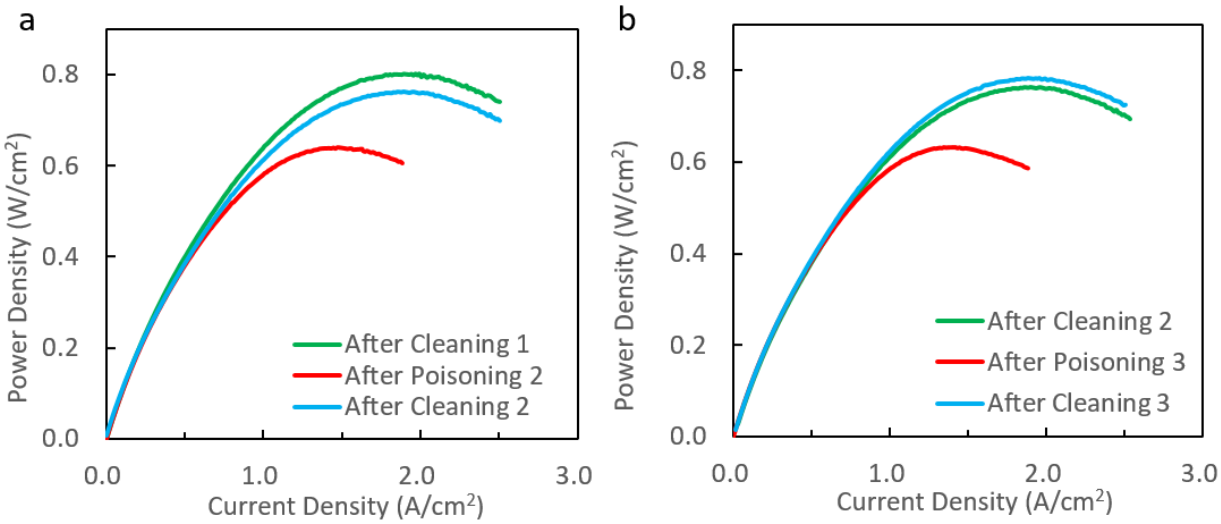

Figure 19. I-V curves for MC-EC after the second (a) and third (b) poisoning-cleaning cycles.

After 25 hours exposure to humidity without the Cr source, the maximum power density of the electrochemical reference cell (MC-REF) increased from 0.96 W/cm^2 to 1.04 W/cm^2, which can be explained by cell activation (Figure 20). The difference of maximum power density between the reference cell and the poisoned cells confirms that degradation in MC-PB & MC-EC were due to Cr poisoning.

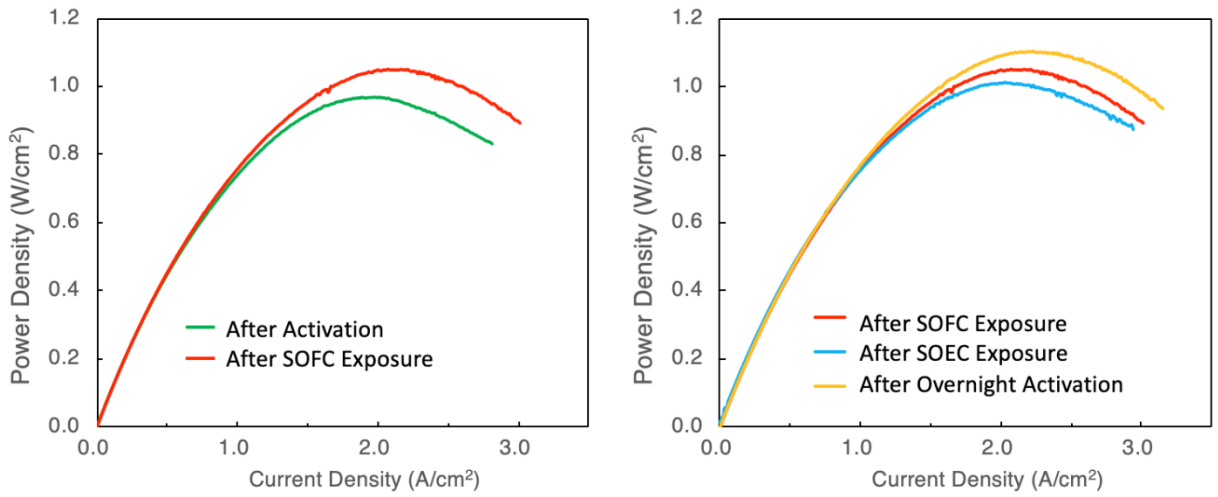

Figure 20. I-V curves for the electrochemical reference cell (MC-REF) a) after activation and after SOFC exposure, and (b) after SOFC exposure, after SOEC exposure, and after overnight activation.

After subjecting MC-REF to electrolytic (electrochemical cleaning) conditions, the maximum power density decreased slightly. However, following overnight activation (10 hours under 0.5 A/cm^2 current density, dry air on the air electrode and 2% humidified H_2 on the fuel electrode), cell performance recovered and was better than before exposure to electrolytic conditions. Again, this demonstrates the reactivation effect observed in LSM-based cells after application of an anodic bias.

The air electrode/electrolyte in MC-PB is covered with Cr deposits (Figure 21.a). However, the concentration of faceted deposits in MC-PB, poisoned for 25 hours, appears to be significantly less than that cell poisoned for 120 hours (Figure 9.a). This again demonstrates the potential to clean before considerable formation of Cr, Mn spinel. It should be noted that the poisoning condition is quite severe here, with a Cr-source right in the path of the air electrode inlet gas located close to the air electrode surface. It is possible that under significantly milder Cr-poisoning conditions in actual operating SOFCs due to the use of protective coatings and Cr-

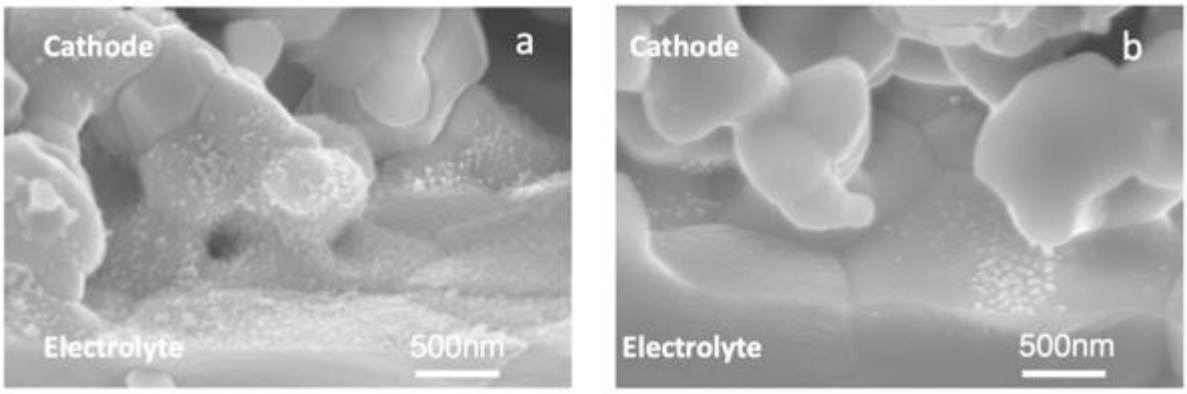

Figure 21. SEM micrographs of air electrode/electrolyte interface of (a) MC-PB after Cr-poisoning, and (b) MC-EC after three cycles of electrochemical cleaning.

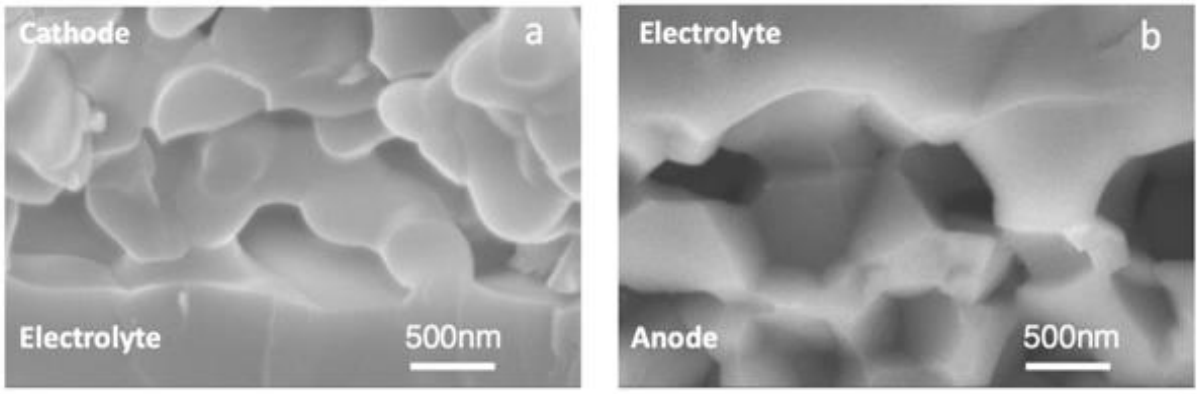

Figure 22. SEM micrograph of MC-REF (a) the air electrode/electrolyte interface and (b) the fuel electrode /electrolyte interface.

getters, formation of Cr, Mn spinel will be delayed to much longer times. Thus, periodic electrochemical cleaning before Cr, Mn spinel formation commences may be a practical pathway to complete cleaning that does not need to occur too frequently.

Figure 21.b shows a SEM micrograph of MC-EC after three cycles of poisoning and cleaning. The interface appears to be relatively clean, with only a few clustered particles visible. EDS analysis showed that these deposits are not Cr species. They could be decomposed air electrode materials. Figure 22 shows that, in general, the air electrode/electrolyte and fuel

electrode/electrolyte interfaces are clean in MC-REF. No delamination was observed at either interface, which shows that electrochemical cleaning under the mild electrolytic condition used here SOEC mode does not damage the cell microstructure.

Task 9: Demonstrate cleaning targets on test cells and cells manufactured by commercial vendors

This task was not directly accomplished. However, using a more realistic Cr source (decreased rate of Cr deposition) including diffusion resistant spinel coatings, in conjunction with complete cell performance recovery via electrochemical cleaning, we are confident that the rate of degradation would be greatly reduced.

Additional Insights A: Demonstration of cleaning on MIEC based cells

Electrochemical cleaning on cells with other air electrode materials, particularly ones that are MIEC, was not investigated in this project. The electrochemical cleaning method is effective when the mechanism of Cr poisoning is itself electrochemical in nature. Poisoning in LSM-based cells has been shown to be significantly impacted by current density. Given appropriate cleaning intervals, removal of Cr-rich deposits is possible for full performance recovery. However, the mechanisms of Cr poisoning in other types of air electrodes appear to be less electrochemically dominant.

For example, previous tests demonstrate a significant improvement in Cr tolerance in LSF-based cells compared to LSM (Figure 23) [2]. These results combined with post-test SEM and EDS analyses provide insight into the mechanisms of Cr deposition in LSF cells (Figure 24). In both air environments, we observe the formation of Sr, Cr-based species on the surface of the

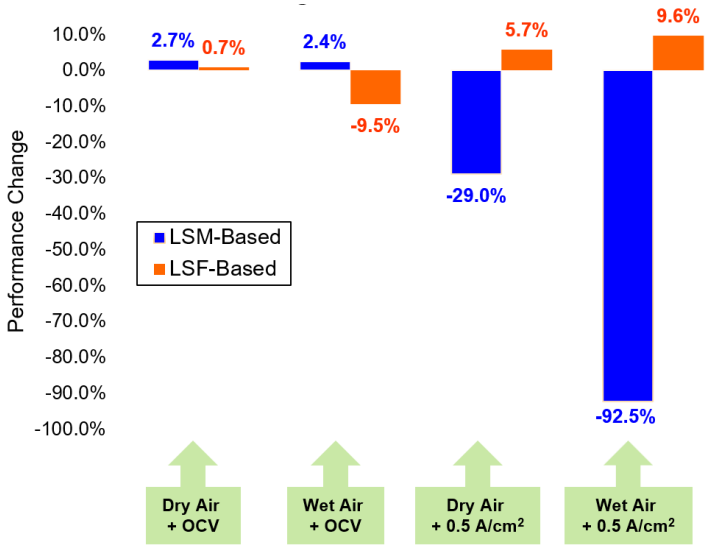

Figure 23. Performance changes over 120 hours exposure to Cr vapor species in LSM and LSF-based cells under varying current densities and air humidities.

air electrode. Chromium preferentially reacts with Sr, which has segregated to the electrode surface, which is typical for LSF-based cells. In the humidified air condition, we also suspect some "chemical cleaning" to be taking place simultaneously. The addition of water vapor in the air increases the partial pressures of Cr vapor species. This results in the vaporization of Sr, Cr-rich deposits from the electrode surface forming Cr and Sr hydroxyl vapor species over the course of 120 hours compared to the cell operated in dry air. Over the course of the study, the loss of Sr from the LSF electrode was not observed to effect cell performance but may be an issue in long term operation.

The addition of humidity also caused the deposition of Cr_2O_3 in the GDC barrier layer. However, we theorize that the level of Cr deposition in this area is limited due to the following mechanism (Figure 25). The solubility of protons in doped CeO_2 is 2 orders of magnitude greater than that in YSZ [7]. When humidified air is supplied over the air electrode, the concentration of protons in GDC is expected to increase due to water uptake. The increased concentration of protons in GDC impede the reduction of hexavalent Cr vapor species, through evaporation of Cr_2O_3 (s) at TPB's via the following reaction:

$$Cr_2O_3\,(s) + 3O_2\,(g) + 6H^+ + 6e^- = 2CrO_2(OH)_2\,(g) + H_2O\,(g)$$

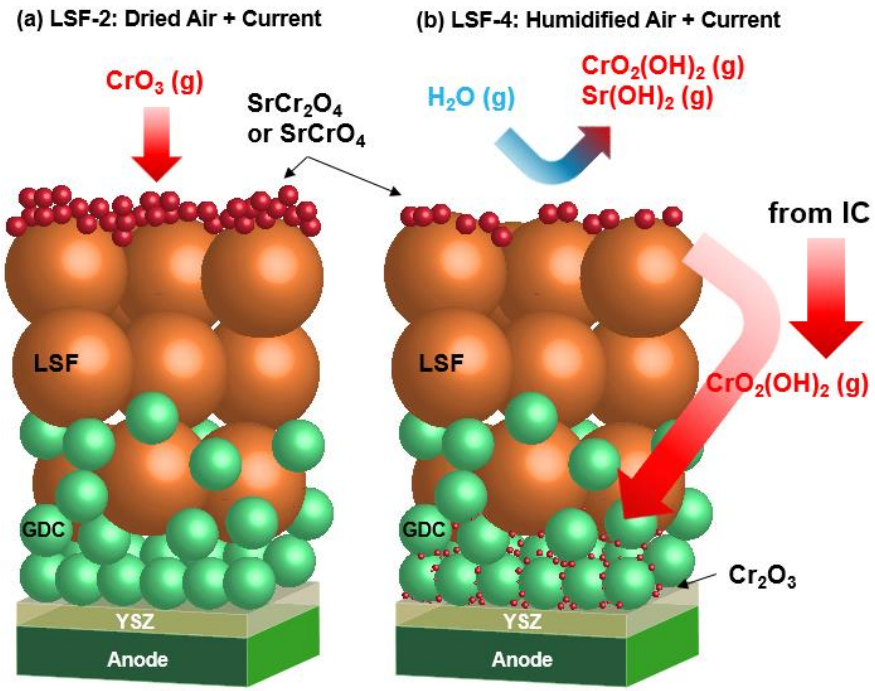

Figure 24. Proposed Cr poisoning mechanisms under dry (a) and humidified (b) air for LSF-based cells.

Due to these differences in phenomena occurring in LSM and LSF-based cells in the presence of Cr vapor species, the electrochemical cleaning method was not investigated in LSF-

based cells. LSF-based cells demonstrate much greater tolerance to Cr deposition. Since LSF is MIEC, Cr poisoning is not mainly electrochemical in nature as is the case for LSM-based cells. Another MIEC electrode material of interest, LNO, that was investigated by our team, similarly demonstrates a much higher tolerance to Cr poisoning compared to LSM-based cells [8]. An LNO-based cell was operated at 800C under 0.5 A/cm^2 for 120h in contact with a Crofer22H mesh. Figure 26 shows the distribution of Cr as a function of distance from the GDC barrier layer through the LNO air electrode. Similar to LSF, the majority of Cr deposition occurs at the surface of the air electrode and some deposition occurs near the interface with GDC. Enrichment of Cr at the surface is chemical in nature forming $LaNi_{0.7}Cr_{0.3}O_3$ perovskite phase and thus won't be greatly affected by electrochemical cleaning. However, at the electrode/barrier layer interface, Cr deposition is suggested to be electrochemical in nature. Assuming that Cr deposition at the interface involves the electrochemical deposition of Cr_2O_3, electrochemical cleaning may be effective here. However, an improvement in cell performance as a result of Cr

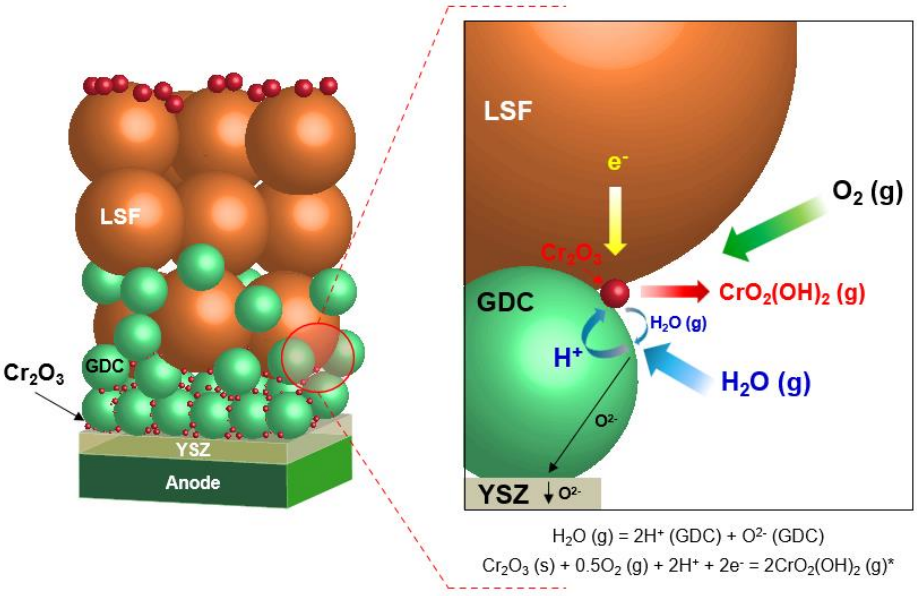

Figure 25. Interaction between doped-ceria phase and humidity in LSF-based cells.

removal in LNO-based cells would not be nearly as a significant as for LSM-based cells, due to the increases TPB lengths in MIEC cells. Perhaps Cr removal may make a difference at much longer time scales if Cr deposition significant impacts pore sizes.

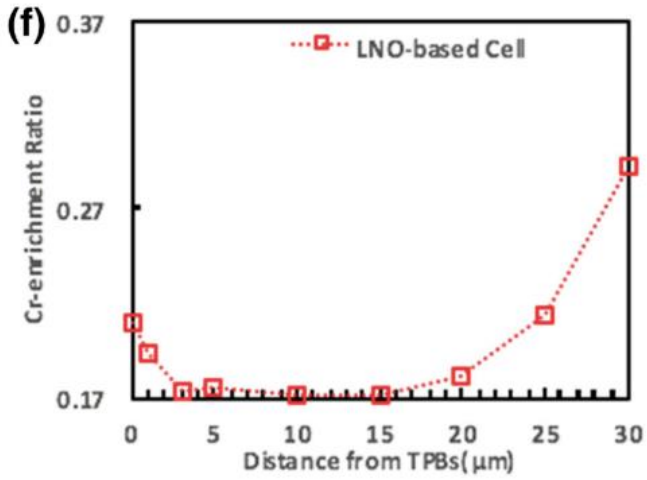

Figure 26. Cr ratio as a function of distance from the GDC barrier layer into an LNO-based cell after 120 hours operation at 0.5 A/cm^2 in direct contact with a Crofer22H mesh. [8]

Additional Insights B: Impact of silver on Cr deposition in LSM-based cells

An additional insight into Cr poisoning and mitigation was made over the course of the project. It was found that a thin layer of silver deposition on the YSZ electrolyte surface prevented significant Cr deposition.

The migration of silver from the mesh and paste used to make electrical connection is often observed in cells when operated under galvanic current. In this case, a large amount of silver paste was applied directly onto the electrode. This resulted in a <1 um layer of silver on the surface of the electrolyte (Figure 27). There was very little to no Cr found in this sample. Comparing the amount of silver and chromium found at the air electrode/electrolyte interface, we observe a threshold value above which Cr deposition appears to be suppressed (Figure 29). The amount of silver migration was reduced by painting the Ag paste onto the Ag mesh (as opposed to the air electrode itself). This also necessitated spring loading onto the mesh to ensure good contact.

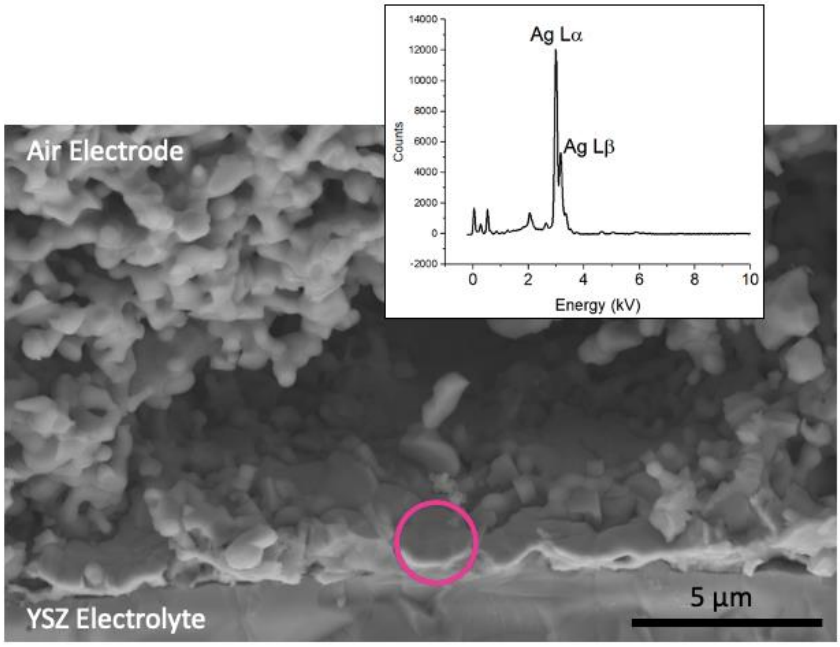

Figure 27. SEM micrograph of air electrode/electrolyte interface. The electrolyte surface was found to be covered with silver deposits.

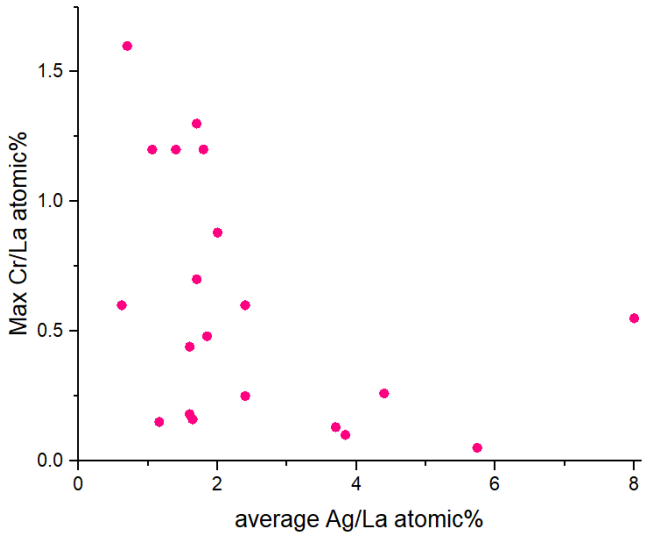

Figure 28. Effect of Ag migration on Cr deposition at the electrode/electrolyte interface in LSM-based cells.

We theorize that due to the high oxygen solubility of silver, oxygen is able to diffuse through the silver layer and reduce at the silver/YSZ interface (Figure 29). In this way, hexavalent Cr vapor species are blocked from reducing at the electrochemically active sites. Unfortunately, this exact method (application of silver onto the electrode surface) does not

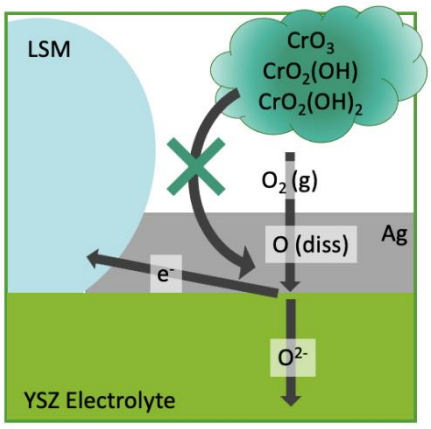

Figure 29. Proposed mechanism of Cr deposition suppression due to Ag coverage on YSZ electrolyte surface.

present a viable Cr poisoning mitigation method as the cell performance also dropped, most likely due to the added process of oxygen migration through the silver layer. However, in the future, application of a very thin silver layer prior to addition of an LSM-based electrode may result in better cell performance while still preventing the deposition of Cr, which in our experience preferentially deposits on the YSZ electrolyte surface.

Conclusions

In summary, this project has clearly demonstrated the efficacy of electrochemical cleaning on chromium removal in LSM-based cells. This was evidenced by performance recovery using current-voltage curves as well as post-test chromium quantification comparison between a cell that was a poisoned and a cell that was poisoned and then cleaned. Multiple poisoning and cleaning cycles showed that cells can be safely subjected to multiple instances of electrochemical cleaning. Cells tests also demonstrated that the Cr, Mn spinel form later in time compared to the Cr oxide and that electrochemical cleaning is effective in removing Cr oxide but not the spinel. This yields the suggestion to clean the cells at an interval that prevents the formation of a significant amount of the spinel for full Cr removal and performance recovery. With the proper interval and in conjunction with Cr-diffusion resistance interconnect coatings, electrochemical cleaning can be employed periodically in order to greatly extend the lifetime of the cell. The project also yielded an investigation into the effect of silver migration on Cr poisoning and development of a new quantification method to capture the distribution of Cr-rich deposits in porous air electrodes. The work of our group also yields insights into the application of electrochemical cleaning to other more Cr-tolerant air electrode materials.

Bibliography

[1] Wang, R., Pal, U. B., Gopalan, S. & Basu, S. N. Chromium Poisoning Effects on Performance of (La,Sr)MnO 3-Based Cathode in Anode-Supported Solid Oxide Fuel Cells. *J. Electrochem. Soc.* **164**, 740–747 (2017).

[2] Wang, R., Sun, Z., Lu, Y., Gopalan, S. & Basu, S. N., Pal, U. B. Comparison of chromium poisoning between lanthanum strontium manganite and lanthanum strontium ferrite composite cathodes in solid oxide fuel cells. *J. Power Sources* **476**, 228743 (2020).

[3] Wang, R., Sun, Z., Pal, U. B., Gopalan, S. & Basu, S. N. Mitigation of chromium poisoning of cathodes in solid oxide fuel cells employing $CuMn_{1.8}O_4$ spinel coating on metallic interconnect. *J. Power Sources* **376**, 100–110 (2018).

[4] Zhu, Z., Sugimoto, M., Pal, U., Gopalan, S. & Basu, S. Electrochemical cleaning: An in-Situ method to reverse chromium poisoning in solid oxide fuel cell cathodes. *J. Power Sources* **471**, (2020).

[5] Huber, A. K., Falk, M., Rohnke, M., Luerssen, B., Amati, M., Gregoratti, L., Hesse, D., Janek, J. In situ study of activation and de-activation of LSM fuel cell cathodes - Electrochemistry and surface analysis of thin-film electrodes. *J. Catalysis* **294**, 79–88 (2012).

[6] Zhu, Z., Sugimoto, M., Pal, U., Gopalan, S. & Basu, S. Multiple cycle chromium poisoning and in-situ electrochemical cleaning of LSM-based solid oxide fuel cell cathodes. *J. Power Sources Adv.* **6**, (2020).

[7] Yokokawa, H. Thermodynamic and SIMS analyses on the role of proton/water in oxygen reduction process and related degradations in solid oxide fuel cells. *Solid State Ionics* **225**, 6–17 (2012).

[8] Gong, Y., Wang, R., Banner, J., Basu, S., Pal, U. B., Gopalan, S. Improved Tolerance of Lanthanum Nickelate ($La_2NiO_{4+\delta}$) Cathodes to Chromium Poisoning Under Current Load in Solid Oxide Fuel Cells. *JOM* **71**, 3848–3858 (2019).

Resulting Publications

Zhu, Z., Sugimoto, M., Pal, U., Gopalan, S. & Basu, S. Electrochemical cleaning: An in-Situ method to reverse chromium poisoning in solid oxide fuel cell cathodes. *J. Power Sources* **471**, (2020).

Zhu, Z., Sugimoto, M., Pal, U., Gopalan, S. & Basu, S. Multiple cycle chromium poisoning and in-situ electrochemical cleaning of LSM-based solid oxide fuel cell cathodes. *J. Power Sources Adv.* **6**, (2020).

Sugimoto, M., Zhu, Z., Gopalan, S., Basu, S., & Pal, U. Investigating Effects of Operational Parameters on the Rate of Electrochemical Cleaning of Chromium Deposits on Strontium-doped Lanthanum Manganite Cathodes in Solid Oxide Fuel Cells. *ECS Meeting Abstracts* **103**, (2021).

Patents

No patents resulted from this work.

Theses

Two theses will be published using parts of this work (Michelle Sugimoto and Zhikuan Zhu) both in May 2022.